REGULAR ARTICLE

The sphericity of the diverse 10-vertex polyhedra found in bare post-transition metal clusters: germanium clusters with interstitial magnesium atoms as model systems

M. M. Uţă · D. Cioloboc · I. Silaghi-Dumitrescu ·
R. B. King

Abstract The diverse polyhedra found experimentally in bare 10-vertex centered post-transition element clusters characterized structurally by X-ray crystallography include the D_{4d} bicapped square antiprism $Zn@In_{10}^{8-}$ in the inter-metallic $K_8In_{10}Zn$ as well as the centered lead clusters $M@Pb_{10}^{2-}$ in $[K(2,2,2-crypt)]_2[M@Pb_{10}]$ (M = Ni, Pd, Pt), the C_{3v} tetracapped trigonal prism $M@In_{10}^{10-}$ in the intermetallic $K_{10}In_{10}M$ (M = Ni, Pd, Pt), the D_{5d} pentagonal antiprism $Pd@Bi_{10}^{4+}$ in $Bi_{14}PdBr_{16}$, and the D_{5h} pentagonal prism in the trianions $M@Ge_{10}^{3-}$ (M = Fe, Co). The structures of the 10-vertex germanium clusters containing an interstitial magnesium atom (atomic radius 1.30 Å), namely $Mg@Ge_{10}^z$ ($z = +2, 0, -2, -4$), have been optimized as models to analyze the frontier molecular orbitals of the four experimentally known 10-vertex polyhedra noted above. In this connection, the molecular orbital patterns of the most spherical D_{4d} bicapped square antiprism cluster $Mg@Ge_{10}$ as well as that of an approximately spherical C_{3v} cluster $Mg@Ge_{10}^{2+}$ derived from the tetracapped trigonal prism exhibit the spherical harmonic ordering of the jellium model. In this ordering scheme, the 20-orbital {1s, 1p, 1d, 2s, 1f, 2p} shell is filled before any of the 1g molecular orbitals. However, the molecular orbital patterns of the oblate D_{5d} pentagonal antiprism cluster $Mg@Ge_{10}^{4-}$ and the D_{5h} pentagonal prism cluster $Mg@Ge_{10}$ no longer exhibit the spherical harmonic ordering of the jellium model. In these clusters, the polar $1f(z^3)$ orbital is raised to antibonding levels and the pair of hexagonal prism g molecular orbitals become bonding orbitals.

Silaghi-Dumitrescu: Deceased December 25, 2009.

M. M. Uţă · D. Cioloboc · I. Silaghi-Dumitrescu
Faculty of Chemistry and Chemical Engineering,
Babeş-Bolyai University, Cluj-Napoca, Romania

R. B. King (✉)
Department of Chemistry, University of Georgia,
Athens, GA 30602, USA
e-mail: rbking@chem.uga.edu

1 Introduction

Modern work on bare post-transition element clusters began in the 1960s after Corbett and co-workers found ways to obtain crystalline derivatives of these post-transition element clusters by use of suitable counterions. Thus crystalline derivatives of the cluster anions have cryptate or polyamine complexed alkali metals as counter-cations [1]. Similarly, crystalline derivatives of the cluster cations have counter-anions, such as $AlCl_4^-$ derived from metal halide strong Lewis acids [2]. With crystalline derivatives of these clusters available, their structures could be determined definitively using X-ray diffraction.

These initial structural studies of such clusters suggested an analogy with the polyhedral boranes, the chemistry of which was developing concurrently. The borane dianions $B_nH_n^{2-}$ and isoelectronic carboranes $CB_{n-1}H_n^-$ and $C_2B_{n-2}H_n$ having $2n + 2$ skeletal electrons ($6 \leq n \leq 12$) were found to exhibit structures based on the "most spherical" deltahedra, that is, polyhedra with all triangular faces and with the vertices having as similar degrees as possible [3]. For the most stable boranes this means having
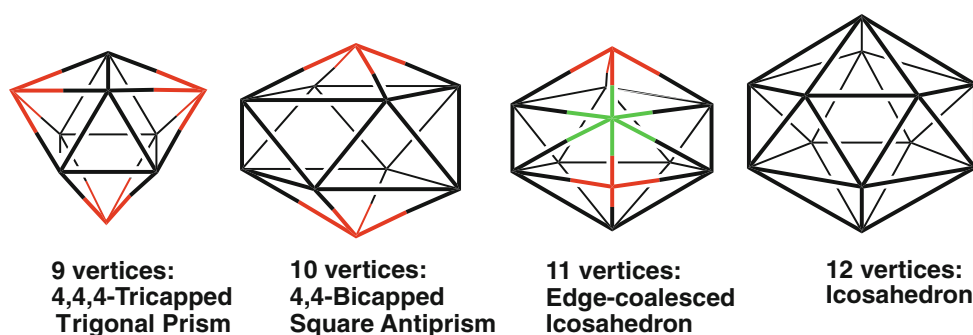
Fig. 1 The "most spherical" deltahedra having from 9 to 12 vertices. Degree 4, 5 and 6 vertices are *red*, *black* and *green*, respectively

9 vertices:
4,4,4-Tricapped
Trigonal Prism

10 vertices:
4,4-Bicapped
Square Antiprism

11 vertices:
Edge-coalesced
Icosahedron

12 vertices:
Icosahedron

as many degree 5 vertices as possible, where the degree of a vertex is the number of edges meeting there. Figure 1 shows the most spherical deltahedra having from nine to 12 vertices. The "ideal" deltahedron for a borane is seen to be the regular icosahedron, which has 12 vertices, all of the optimum degree 5. Thus $B_{12}H_{12}^{2-}$ with an icosahedral structure is the most stable and least reactive of the $B_nH_n^{2-}$ boranes. The rules correlating the shape of polyhedral boranes with the skeletal electron count were first observed by Williams [3] and developed further by Wade [4, 5] and then Mingos [6, 7]. They have subsequently become known as the Wade–Mingos rules.

As the chemistry of bare post-transition element clusters developed further, limitations in this analogy between such clusters and polyhedral boranes became increasingly apparent. The most dramatic example occurs with the icosahedral systems, where icosahedral E_{12}^{2-} (E = Si, Ge, and Sn) isoelectronic analogs of the very stable $B_{12}H_{12}^{2-}$ remain essentially unknown. The reason for this major difference was discovered [8] when $B_{12}H_{12}^{2-}$ was found to be aromatic but the isoelectronic and still unknown Si_{12}^{2-} to be antiaromatic using the nucleus independent chemical shifts (NICS) test for aromaticity developed by Schleyer and collaborators [9].

In order to understand the underlying reasons for differences in the structures between analogs boranes and post-transition element clusters, we initiated in 1999 a density functional theory (DFT) study of such clusters with particular focus on bare germanium clusters. Such studies included the species Ge_n^z ($5 \leq n \leq 12$ and $n = 14$) [10–16] with even charges bracketing the $2n + 2$ skeletal electron Ge_n^{2-} systems in both the hyperelectronic ($z < -2$) and hypoelectronic ($z \geq 0$) directions. Germanium was chosen as the element for our studies in order to minimize the charges in species with the skeletal electron counts of interest. In this connection note that the Wade–Mingos rules [4–7] consider bare germanium vertices to have an external lone pair so that each germanium vertex is a donor of two skeletal electrons similar to a BH vertex in the polyhedral boranes.

In some cases our DFT studies predicted lowest energy structures for Ge_n^{2-} clusters that are different from the well-
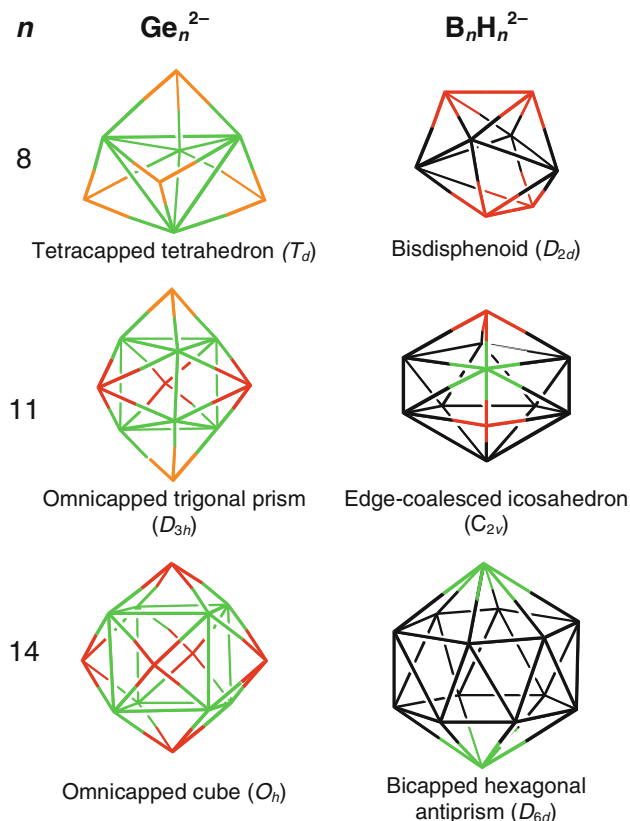
n	Ge_n^{2-}	$B_nH_n^{2-}$

8

Tetracapped tetrahedron (T_d)

Bisdisphenoid (D_{2d})

11

Omnicapped trigonal prism (D_{3h})

Edge-coalesced icosahedron (C_{2v})

14

Omnicapped cube (O_h)

Bicapped hexagonal antiprism (D_{6d})

Fig. 2 Examples of different lowest energy structures for isoelectronic Ge_n^{2-} and $B_nH_n^{2-}$ derivatives ($n = 8, 11, 14$). Degree 3, 4, 5 and 6 vertices are *orange*, *red*, *black* and *green*, respectively

established structures of the isoelectronic boranes $B_nH_n^{2-}$ and carboranes $CB_{n-1}H_n^-$ and $C_2B_{n-2}H_n$ (Fig. 2). Thus the lowest energy structure for Ge_8^{2-} is a T_d tetracapped tetrahedron whereas that for $B_8H_8^{2-}$ is a D_{2d} bisdisphenoid. Similarly the lowest energy structure for Ge_{11}^{2-} is a D_{3h} pentacapped trigonal prism whereas that for $B_{11}H_{11}^{2-}$ is a C_{2v} deltahedron. For Ge_{14}^{2-} the structure greatly preferred energetically is a very symmetrical O_h omnicapped cube whereas that for $B_{14}H_{14}^{2-}$ and observed experimentally [17] in a carborane of the type $R_2C_2B_{12}H_{12}$ is a D_{6d} bicapped hexagonal antiprism. Note that the favored borane structures maximize the numbers of degree 5 vertices

(black vertices in Fig. 2), whereas for the germanium clusters degree 5 vertices appear to be less favorable than degree 4 and 6 vertices (red and green vertices in Fig. 2). Thus none of the lowest energy Ge_n^{2-} dianion structures ($n = 8, 11, 14$) have even a single degree 5-vertex.

These limitations in the Wade–Mingos rules [4–7] to predict the structures of bare post-transition element clusters motivated the use of an alternative approach [18] to understand such structures based on the jellium model [19, 20] for spherical clusters. Mingos and collaborators [21–23] have also recognized limitations of the original Wade–Mingos rules when applied to spherical bare metal clusters. Thus they have used the jellium model to understand the structure and bonding in phosphine gold clusters [23]. Such methods also relate to the success of Stone's tensor surface harmonic theory [24–26].

The jellium model arises from the recognition of certain bare spherical free-electron metal clusters as "superatoms" among which the 40 total valence electron species Al_{13}^-, observed in gas phase experiments [27], is the prototypical example. However, whereas in an atom the positive charge of a nucleus is concentrated at a central point, in a cluster the positive charge can be assumed to be distributed over a positive ion core the size of the cluster leading to a so-called jellium sphere. Both situations lead to discrete electronic energy levels. However, the different distributions of the positive charges lead to different ordering of the electronic energy levels and thus to different closed shell configurations (Fig. 3). Thus for atoms the closed shell configurations have 2, 10, 18, 36, 54 and 86 electrons corresponding to the noble gases, which are the least chemically reactive of all of the elements. However, for the jellium model the closed shell configurations relevant to cluster chemistry are those with 20 and 40 total valence electrons.

An example of a stable well-known cluster with 20 total valence electrons is white phosphorus, P_4. Examples of clusters with 40 total valence electrons are Al_{13}^- found in gas phase experiments [27], In_{11}^{7-} found in the intermetallic [28] K_8In_{11}, and Ge_9^{4-} obtained from dissolution of A_4Ge_9 alloys (A = alkali metal) in liquid ammonia. Stable 40 total valence electron clusters with interstitial atoms are also known such as $M@In_{10}^{10-}$ in the $K_{10}In_{10}M$ intermetallics (M = Ni, Pd, Pt) [29] and $Zn@In_{10}^{8-}$ in the $K_8In_{10}Zn$ intermetallic [30]. In counting the total valence electrons in such bare post-transition element clusters the "external lone pairs" of the Wade–Mingos model are now counted among the total valence electrons so that Al, Ga, In and Tl vertices contribute all three of their valence electrons and Si, Ge, Sn and Pb contribute all four of their valence electrons. However, the filled d^{10} shells of interstitial atoms are not considered as valence electrons. Thus the interstitial nickel atom in $Ni@In_{10}^{10-}$ is a donor of zero valence electrons and can even be considered as a pseudo noble gas
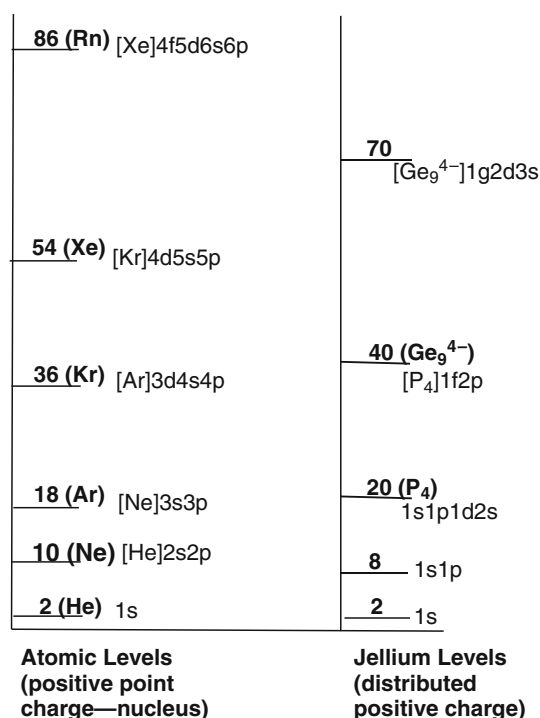

Fig. 3 A comparison of the electronic energy levels in an atom and a jellium sphere

[31]. Similarly the interstitial zinc atom in $Zn@In_{10}^{8-}$ is a donor of two valence electrons.

The 10-vertex systems are the focus of this research because of the variety of polyhedra found in structures that have been realized experimentally and characterized by X-ray diffraction. Thus four different 10-vertex bare post-transition element polyhedra have been found to host interstitial guest atoms in $M@E_{10}$ structures (Fig. 4). A D_{4d} bicapped square antiprism is found to encapsulate a group 10 metal atom in the anionic indium cluster $Zn@In_{10}^{8-}$ found in the intermetallic [30] $K_8In_{10}Zn$ as well as the lead clusters $M@Pb_{10}^{2-}$ in $[K(2,2,2-crypt)]_2[M@Pb_{10}]$ (M = Ni, Pd, Pt) [32, 33]. This polyhedron is the most spherical 10-vertex deltahedron found in polyhedral boranes such as $B_{10}H_{10}^{2-}$ (Fig. 1). However, in the isoelectronic $M@In_{10}^{10-}$ clusters found in the $K_{10}In_{10}M$ intermetallics (M = Ni, Pd, Pt) the encapsulating polyhedron is a C_{3v} tetracapped trigonal prism [29]. The pentagonal antiprism is the host polyhedron for an interstitial palladium atom in the cationic bismuth cluster $Pd@Bi_{10}^{4+}$ in $Bi_{14}PdBr_{16}$ (=$[Pd@Bi_{10}]$ $[BiBr_4]_4$) [34]. The pentagonal prism has been found as the host polyhedron for an iron or cobalt atom in the clusters $M@Ge_{10}^{3-}$ (M = Fe [35], Co [36]). These pentagonal prismatic clusters are particularly unusual since the pentagonal prism has no triangular faces at all but only rectangular and pentagonal faces. This is in stark contrast to the fundamental deltahedra of borane chemistry in which all of the faces are triangles. Furthermore, theoretical studies [37–40]
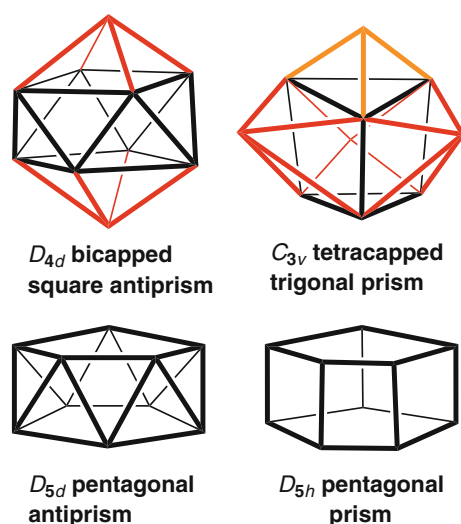
Fig. 4 The four 10-vertex polyhedra found as host polyhedra for interstitial metal atoms. For clarity the edges of degree 3 and 4 capping vertices are shown in *orange* and *red*, respectively

suggest that in some cases the preferred cluster polyhedron for enclosing a central metal atom is simply the polyhedron with the largest internal volume rather than a polyhedron meeting the electronic requirements of the Wade–Mingos rules [4–7]. For the 10-vertex systems this polyhedron is the pentagonal prism with the minimum number of edges and hence no triangular faces.

The jellium model for the chemical bonding in bare post-transition element clusters depends on the approximation of the actual polyhedron by a sphere. The accuracy of this approximation can be tested by the correspondence of the calculated molecular orbital patterns to those suggested in Fig. 3. For this purpose 10-vertex magnesium-centered germanium clusters were used as models for the polyhedra of interest. Magnesium was chosen to be the interstitial atom since it has a single +2 oxidation state so that it is an unambiguous donor of two valence electrons. Thus $Mg@Ge_{10}^{2+}$ clusters are examples of systems with the magic number of 40 total valence electrons, namely two from the central magnesium atoms and four from each germanium atom minus two for the +2 charge.

This paper presents a detailed DFT study on the structures and energetics of the $Mg@Ge_{10}^{z}$ clusters ($z = +2$, 0, -2, -4). In addition, the sphericities of the lowest energy $Mg@Ge_{10}^{z}$ structures based on the four polyhedra in Fig. 4 are examined by comparing the patterns of their bonding molecular orbitals with those expected for a jellium sphere (Fig. 3).

2 Theoretical methods

Geometry optimizations were carried out at the hybrid DFT B3LYP level [41–44] with the 6-31G(d) (valence) double-

zeta quality basis functions extended by adding one set of polarization (d) functions for both the interstitial and germanium atoms. The Gaussian 03 package of programs [45] was used in which the fine grid (75,302) is the default for numerically evaluating the integrals and the tight (10^{-8}) hartree stands as default for the self-consistent field convergence. Computations were carried out using six initial geometries of 10-vertex polyhedra with threefold, fourfold and fivefold symmetry including the four polyhedra in Fig. 1 as well as a prolate C_{3v} structure and the D_{4h} bicapped cube. The symmetries were maintained during the initial geometry optimization processes. Symmetry breaking using modes defined by imaginary vibrational frequencies was then used to determine optimized structures with minimum energies. Vibrational analyses show that all of the final optimized structures discussed in this paper are genuine minima at the B3LYP/6-31G(d) level without any significant imaginary frequencies ($N_{imag} = 0$). In a few cases, the calculations ended with acceptable small imaginary frequencies [46], and these values are indicated in the corresponding figures.

The optimized structures found for the $Mg@Ge_{10}^{z}$ derivatives are labeled by the number of skeletal electrons and their relative energies. Triplet structures are indicated by **T**. Thus the lowest energy structure of singlet neutral $Mg@Ge_{10}$ is labeled **22-1**. Additional details of all of the optimized structures, including all interatomic distances, the initial geometries leading to a given optimized structure and structures with energies too high to be of possible chemical relevance, are provided in the Supporting Information. In assigning polyhedra to the optimized structures, the Ge–Ge distances less than ~3.2 Å were normally considered as polyhedral edges; significant exceptions are noted in the text. Similarly Mg–Ge distances less than ~2.8 Å are considered bonding distances; most such Mg–Ge bonding distances were less than ~2.5 Å except for some of the less regular polyhedra. The magnesium atom is numbered as atom 1 in all of the structures.

For the determination of the bonding molecular orbital patterns of the representative $Mg@Ge_{10}^{z}$ structures exhibiting the four polyhedra in Fig. 4, the symmetries were maintained during the geometry optimization. Details of the molecular orbital energies are given in the Supporting Information.

3 Background

The order of filling of the free electronic states in a jellium sphere is quite different from that of a free atom (Fig. 3) [19]. Whereas in a free atom the 2s level immediately follows the 1s level, in a jellium sphere the 1p and 1d levels follow the 1s level before the 2s level is reached.

Subsequently in the free atom only the 2p level follows the 2s level before the 3s level is reached. However, in the jellium model the 2s level is followed by the 1f, 2p, 1g and 2d levels before the 3s level is reached.

An important difference between the energy level patterns of atoms and jellium spheres is the involvement of f- and g-type orbitals in atoms and in jellium spheres. In atoms the f orbitals only appear when the lanthanides are reached. The f orbitals begin to play a significant chemical role only in the chemistry of the heaviest elements, namely the actinides, many of which are too radioactive with too short half-lives to have much chemical significance. The g orbitals, although interesting mathematically [47], play no role in any real chemistry. However, for jellium clusters (Fig. 3) the 1f molecular orbitals are already involved as bonding orbitals in clusters with the magic 40 total valence electrons, such as Al_{13}^-, In_{11}^{7-} and Ge_9^{4-} discussed above. Furthermore, for clusters with more than 40 total valence electrons or clusters deviating from sphericity, the 1g molecular orbitals can also become bonding orbitals. Since the nature of f and g orbitals is not familiar to chemists some of their important properties will be examined.

The patterns of the f and g orbitals can be seen most readily if the underlying sphere is considered to be the earth with the z-axis running through the north and south poles. Then the single linear f and g orbitals with polynomials containing only z with $m = 0$ can be considered to be polar orbitals (Tables 1, 2). Conversely the pairs of f and g orbitals with polynomials containing only x and y with the maximum value of $|m|$ correspond to a polygon in the equatorial plane and thus can be considered as equatorial orbitals. The orbitals between these extremes can be considered as "tropical," "temperate" and/or "arctic" orbitals by analogies with the climatic zones of the earth. Using this terminology the cube f orbitals with $|m| = 2$ are "tropical" f orbitals and the double square f orbitals with $|m| = 1$ are "temperate" f orbitals. Similarly the intermediate g orbitals (Table 2) can be classified as "tropical," "temperate" and "arctic" for $|m|$ values of 3, 2 and 1, respectively. Note that the tropical orbitals have their lobes oriented toward the vertices of a cube and a hexagonal prism for the f and g orbitals, respectively.

The shapes of f and g orbitals can become very complicated to visualize because of the large number of lobes. A convenient way of depicting the shapes of such orbitals is by the use of an orbital graph [48, 49]. In such an orbital graph the vertices correspond to the lobes of the atomic orbitals and the edges to nodes between adjacent lobes of opposite sign. Such an orbital graph is necessarily a signed bipartite graph in which each vertex is labeled with the sign of the corresponding lobe and only vertices of opposite sign can be connected by an edge. The orbital graphs and polynomials for the seven f orbitals and the nine g orbitals are listed in Tables 1 and 2, respectively.

A polyhedron can be regarded as spherical if its vertices can correspond to points on a sphere where the radii in the x, y and z directions are equivalent (Fig. 5). Initial deviations from sphericity can occur in two directions corresponding to compression or elongation in one direction, conveniently designated as the z-axis. Compression along the z-axis gives an oblate ellipsoid whereas expansion along the z-axis gives a prolate ellipsoid. The borane deltahedra, including the 9-, 10-, 11- and 12-vertex polyhedra in Fig. 1, are examples of essentially spherical polyhedra. Removal of an antipodal pair of vertices from such a polyhedron, for example, conversion of an icosahedron (Fig. 1) to a pentagonal antiprism (Fig. 4), corresponds to a

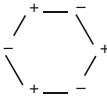**Table 1** Properties of the f atomic or molecular orbitals arising from the spherical harmonics
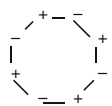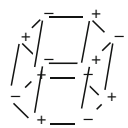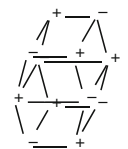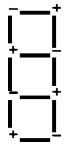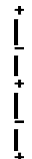
$|m|$	Lobes	Shape	Orbital graph	Polynomial	Type
3	6	Hexagon		$x(x^2 - 3y^2)$ $y(3x^2 - y^2)$	Equatorial
2	8	Cube		xyz $z(x^2 - y^2)$	Tropical
1	6	Double square		$x(5z^2 - r^2)$ $y(5z^2 - r^2)$	Temperate
0	4	Linear		$z(5z^2 - r^2)$	Polar

Table 2 Properties of the g atomic or molecular orbitals arising from the spherical harmonics

$|m|$	Lobes	Shape	Orbital graph	Polynomial	Type
4	8	Octagon		$x^4 + y^4 - 6x^2y^2$ $xy(x^2 - y^2)$	Equatorial
3	12	Hexagonal prism		$xz(x^2 - 3y^2)$ $yz(y^2 - 3x^2)$	Tropical
2	12	Double cube		$(x^2 - y^2)(7z^2 - r^2)$ $xy(7z^2 - r^2)$	Temperate
1	8	Triple square		$y(7z^3 - 3zr^2)$ $x(7z^3 - 3zr^2)$	Arctic
0	5	Linear		$35z^4 - 30z^2r^2 + 3r^4$	Polar

compression along the z-axis so that the pentagonal antiprism is an example of an oblate ellipsoidal polyhedron. Extreme examples of oblate deltahedral clusters are the dirhenaboranes $(\eta^5\text{-Me}_5\text{C}_5)_2\text{Re}_2\text{B}_n\text{H}_n$ ($n = 4, 5, 6, 7, 8$) synthesized by Fehlner and co-workers [50–52] and discussed theoretically elsewhere [53]. The differences between the molecular orbital patterns of spherical and oblate ellipsoidal polyhedra are examined in this paper using the magnesium-centered 10-vertex germanium clusters Mg@Ge_{10}^z as examples.

4 Results and discussion

4.1 Structures and energetics of the Mg@Ge_{10}^z clusters

4.1.1 The dication Mg@Ge_{10}^{2+} (Fig. 6)

The three lowest energy structures of the Mg@Ge_{10}^{2+} dication with 20 skeletal electrons by the Wade–Mingos rules [4–7], namely **20-1**, **20-2** and **20-3**, all have the magnesium atom on the surface of a highly irregular MgGe_{10} polyhedron (Fig. 6). This suggests that these Ge_{10} polyhedra do not have a large enough internal volume to accommodate an interstitial magnesium atom in the center
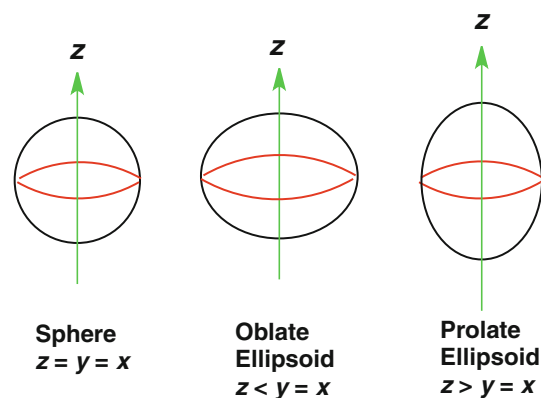
Fig. 5 Comparison of the *sphere*, *oblate ellipsoid* and *prolate ellipsoid* showing the equators in *red* and the polar axis in *green*

of the polyhedron. The lowest energy Mg@Ge_{10}^{2+} structure with an interstitial magnesium atom is **20-4**, lying 45.2 kcal/mol above the global minimum **20-1**. The Ge_{10} polyhedron surrounding the magnesium atom in **20-4** has C_{3v} symmetry with three quadrilateral faces meeting at the unique vertex on the C_3 axis. The other Mg@Ge_{10}^{2+} structure with a true interstitial magnesium atom is the D_{4d} bicapped square antiprismatic structure **20-6** lying 46.0 kcal/mol above the global minimum **20-1**. The sixth

$Mg@Ge_{10}^{2+}$ structure of comparable energy, namely **20-5**, lying 45.9 kcal/mol above **20-1**, has the magnesium atom on the surface rather than in the center of a highly irregular polyhedron and thus resembles the lower energy structures **20-1**, **20-2**, and **20-3**.

4.1.2 The neutral $Mg@Ge_{10}$ (Fig. 7)

The three lowest energy structures of the 22-skeletal electron species $Mg@Ge_{10}$ all have an external Ge_{10} polyhedron surrounding a central magnesium atom (Fig. 7). This differs from the three lowest structures of the dication $Mg@Ge_{10}^{2+}$, namely **20-1**, **20-2** and **20-3**, in which the magnesium atom is on the surface of the polyhedron rather than in the center (Fig. 6). In the lowest energy

$Mg@Ge_{10}$ structure **22-1**, the Ge_{10} polyhedron is the D_{4d} bicapped square antiprism expected for a 22 skeletal electron system in accord with the Wade–Mingos rules (Fig. 7) [4–7]. The next $Mg@Ge_{10}$ structure **22-2T** is a triplet C_{3v} structure lying 8.9 kcal/mol above the global minimum **22-1**. This triplet $Mg@Ge_{10}$ structure is very similar to the singlet structure **20-4** of the dication $Mg@Ge_{10}^{2+}$ (Fig. 6). The final low-energy $Mg@Ge_{10}$ structure **22-3**, lying 13.4 kcal/mol above the global minimum **22-1**, is a D_{5h} pentagonal prismatic structure.

4.1.3 The dianion $Mg@Ge_{10}^{2-}$ (Fig. 8)

Six structures are found for the 24 skeletal electron dianion $Mg@Ge_{10}^{2-}$ within 16 kcal/mol of the global minimum **24-1**

Fig. 6 The six lowest energy $Mg@Ge_{10}^{2+}$ structures
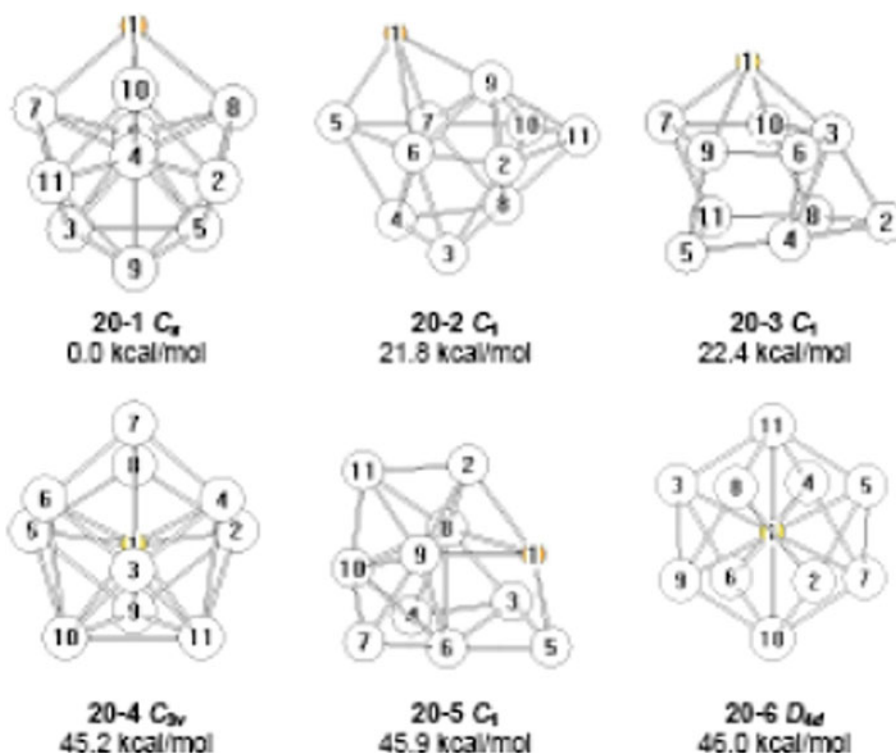
20-1 C_s
0.0 kcal/mol

20-2 C_1
21.8 kcal/mol

20-3 C_1
22.4 kcal/mol

20-4 C_{3v}
45.2 kcal/mol

20-5 C_1
45.9 kcal/mol

20-6 D_{4d}
46.0 kcal/mol

Fig. 7 The three lowest energy $Mg@Ge_{10}$ structures

22-1 D_{4d}
0.0 kcal/mol

22-2T C_{3v}
8.9 kcal/mol

22-3 D_{5h}
13.4 kcal/mol

Fig. 8 The six lowest energy $Mg@Ge_{10}^{2-}$ structures

24-1 C_1
0.0 kcal/mol

24-2 C_s
0.3 kcal/mol

24-3 C_{3v}
5.7 kcal/mol

24-4 C_s
7.3 kcal/mol

24-5 C_s
11.3 kcal/mol

24-6T D_{5d}
15.9 kcal/mol
07I
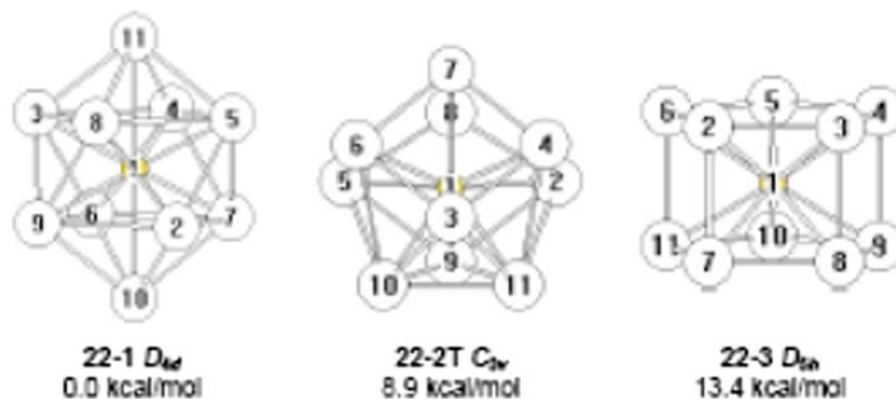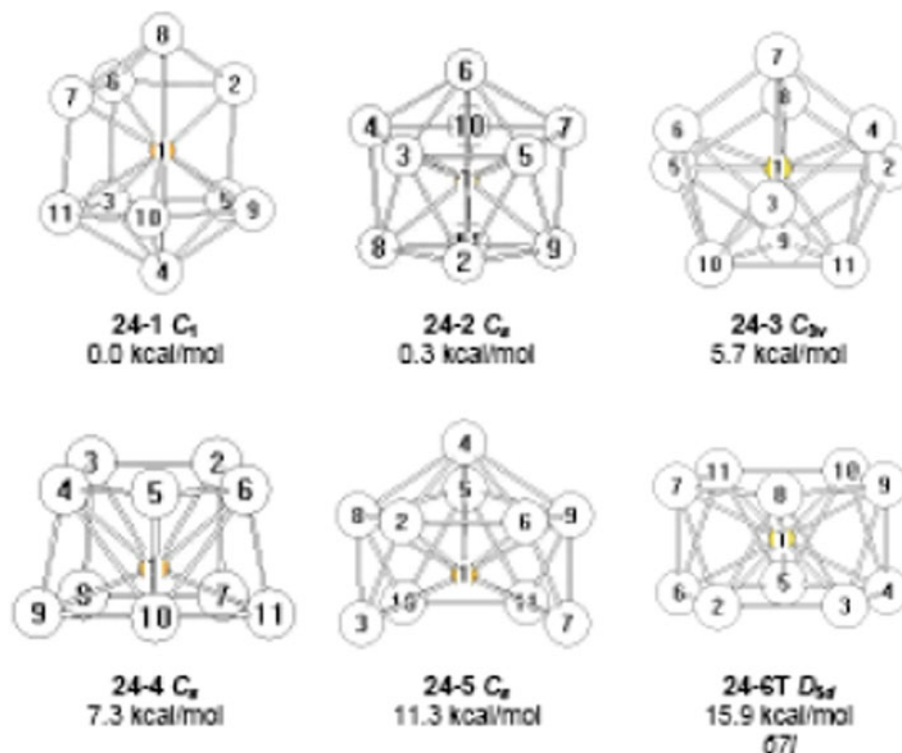
(Fig. 8). This global minimum is an open structure but with the magnesium atom in the center. The external Ge_{10} polyhedron in **24-1** can be derived from a D_{5h} bicapped pentagonal prism by removal of two adjacent vertices from one of the pentagonal faces of the underlying pentagonal prism. The next $Mg@Ge_{10}^{2-}$ structure **24-2** is a C_s structure lying only 0.3 kcal/mol above the global minimum **24-1**. The outer Ge_{10} polyhedron in **24-2** has one rhombus face (Ge2-Ge8-Ge11-Ge9) at the bottom and two more square faces (Ge8-Ge11-Ge10-Ge4; Ge9-Ge11-Ge10-Ge7) as well as 10 triangular faces. The next $Mg@Ge_{10}^{2-}$ structure **24-3**, lying 5.7 kcal/mol above **24-1**, is a singlet C_{3v} polyhedron with three rectangular faces very similar to the triplet $Mg@Ge_{10}$ structure **22-2T**. The $Mg@Ge_{10}^{2-}$ structure **24-4**, lying 7.3 kcal/mol above **24-1**, is essentially a distorted pentagonal prism. The distortion reduces the D_{5h} symmetry of an ideal pentagonal prism to C_s. The $Mg@Ge_{10}^{2-}$ structure **24-5** lies 11.3 kcal/mol above the global minimum **24-1**. The Ge_{10} polyhedron in **24-5** is a relatively open polyhedron that can be derived from a regular icosahedron by removal of two adjacent vertices. The final $Mg@Ge_{10}^{2-}$ structure **24-6T**, lying 15.9 kcal/mol above **24-1**, is a D_{5d} triplet pentagonal antiprism.

4.1.4 The tetraanion $Mg@Ge_{10}^{4-}$ (Fig. 9)

Seven structures were found for the 26 skeletal electron tetraanion $Mg@Ge_{10}^{4-}$ within 30 kcal/mol of the global

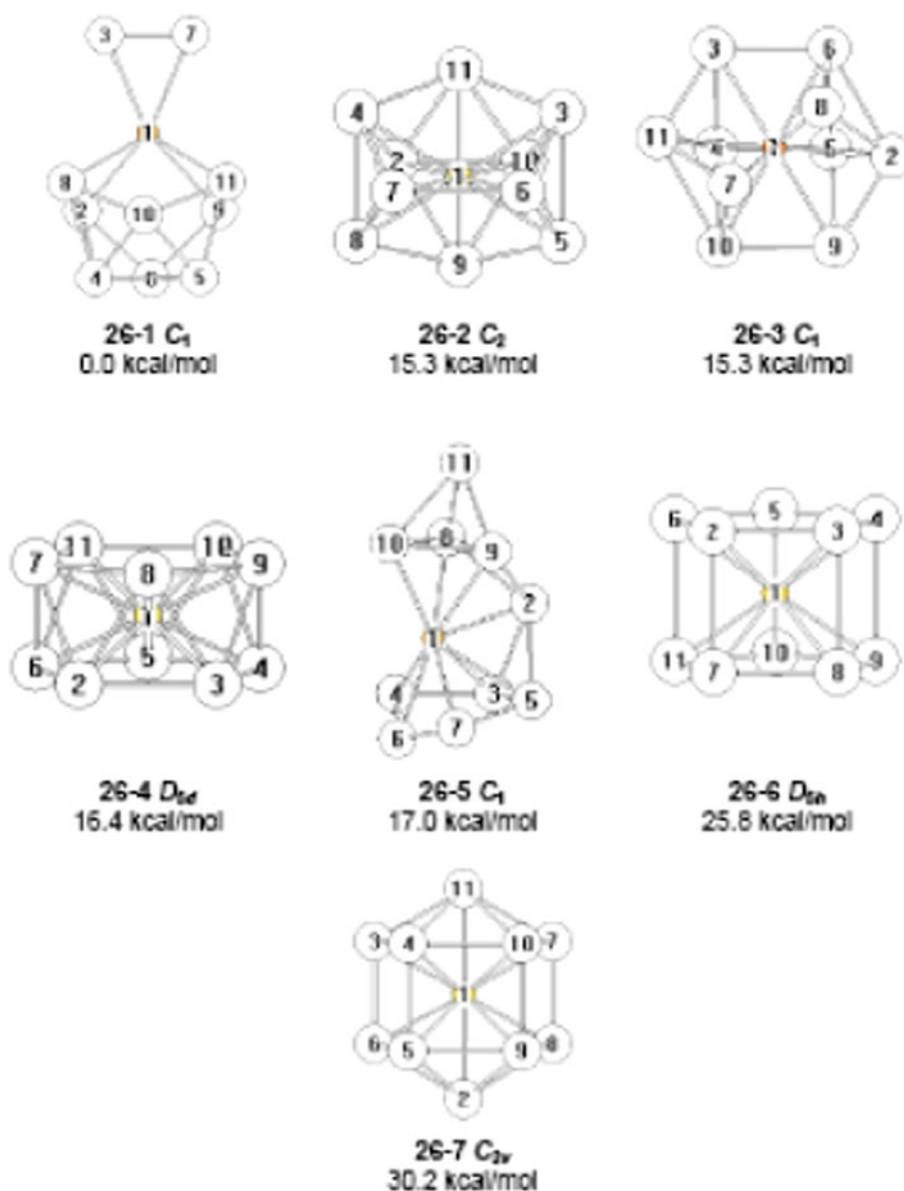minimum **26-1** (Fig. 9). This global minimum **26-1** is an open structure in which the Ge_{10} unit has split into a Ge_2 unit and a Ge_8 unit. The distance between the magnesium atom and the two germanium atoms corresponding to the Ge_2 unit is 2.86 Å. Regarding the Ge_8 unit, the distance between the magnesium atom and two of the nearby germanium atoms, namely Ge8 and Ge11, is 2.70 Å, whereas the distance between the magnesium atom and the other two neighbouring germanium atoms, namely Ge2 and Ge9, is 3.00 Å. The latter can be considered a nonbonding distance. The Ge10 atom lies 3.21 Å from the magnesium atom.

The lowest energy closed polyhedral $Mg@Ge_{10}^{4-}$ structure **26-2** lies 15.3 kcal/mol above the global minimum **26-1** suggesting that the Mg atom is too large to fit into a Ge_{10}^{4-} unit. The Ge_{10} polyhedron in **26-2** has two vertices of degree 3, six vertices of degree 4 and two vertices of degree 5. This polyhedron is similar to the pentagonal antiprism since it has two pentagonal faces as well as ten triangular faces but is considerably less symmetrical. The presence of two open pentagonal faces in **26-2** is consistent with the Wade–Mingos rules [4–7] for this system with 26 ($=2n + 6$ for $n = 10$) skeletal electrons.

Another relatively open polyhedron is found in the next $Mg@Ge_{10}^{4-}$ tetraanion structure **26-3**, which is essentially degenerate with **26-2**, since it also lies 15.3 kcal/mol above **26-1**. Structure **26-5**, lying 26.0 kcal/mol above

Fig. 9 The seven lowest energy $Mg@Ge_{10}^{4-}$ structures

26-1 C_1
0.0 kcal/mol

26-2 C_2
15.3 kcal/mol

26-3 C_1
15.3 kcal/mol

26-4 D_{5d}
16.4 kcal/mol

26-5 C_1
17.0 kcal/mol

26-6 D_{5h}
25.8 kcal/mol

26-7 C_{2v}
30.2 kcal/mol

26-1, is an even more open structure. The magnesium atom in **26-5** is situated less than 2.8 Å from only three germanium atoms. The distance from the magnesium atom to six of the other seven germanium atoms falls between 2.81 and 2.99 Å, while the distance from the magnesium to Ge11 is 4.41 Å.

The remaining three $Mg@Ge_{10}^{4-}$ structures are all well-defined polyhedra. Thus structure **26-4**, lying 16.4 kcal/mol above **26-1**, is clearly an undistorted D_{5d} pentagonal antiprism. Structure **26-6**, lying 25.8 kcal/mol above **26-1**, is an undistorted D_{5h} pentagonal prism. The Ge_{10} polyhedron in **26-7**, lying 30.2 kcal/mol above **26-1**, has a large hexagonal face in addition to three rectangular faces and six triangular faces. It has six degree 4 vertices and four degree 3 vertices.

4.2 Molecular orbitals of representative $Mg@Ge_{10}^{z}$ clusters

4.2.1 Spherical polyhedra

The first polyhedron chosen for this study was the D_{4d} bicapped square antiprism (Figs. 4, 10). This polyhedron is the most spherical deltahedron found in boranes such as $B_{10}H_{10}^{2-}$ and thus might be expected to be the 10-vertex polyhedron most closely approximated by a sphere. Neutral $Mg@Ge_{10}$ with 42 total valence electrons (structure **22-1** in Fig. 7) was chosen for the D_{4d} structure since it is iso-electronic with the known $B_{10}H_{10}^{2-}$. Since 42 is two more than the closed shell configuration of 40 total electrons (Fig. 3) a spherical harmonic ordering of the bonding

molecular orbitals first fills the 1s, 1p, 1d, 2s, 1f and 2p shells leaving two electrons for a 1g HOMO. This indeed is found to be the case for D_{4d} Mg@Ge$_{10}$ (Fig. 10). Thus the HOMO is the polar $1g(z^4)$ orbital (Table 2), which becomes the lowest energy g orbital because of the two vertices on the z-axis (i.e., the C_4 axis) of the bicapped square antiprism. Also in D_{4d} Mg@Ge$_{10}$ the lowest lying f molecular orbital is the polar $1f(z^3)$ orbital and the lowest lying d molecular orbital is the polar $1d(z^2)$ orbital. Thus the spherical harmonic ordering of molecular orbitals in

D_{4d} Mg@Ge$_{10}$ demonstrates the most spherical nature of the D_{4d} bicapped square antiprism.

The molecular orbital pattern of D_{4d} Mg@Ge$_{10}$ also shows the difference between the 1s and 2s molecular orbitals. Thus the 1s molecular orbital (the lowest lying orbital in Fig. 10) has neither radial nor angular nodes. However, the 2s molecular orbital clearly has a radial node at the surface of the deltahedron. This is depicted in Fig. 10 by the inside of the orbital being colored gray and the outside of the orbital being colored blue. Similar radial

Fig. 10 The bonding molecular orbitals for the 42 total electron D_{4d} bicapped square antiprismatic Mg@Ge$_{10}$ structure (structure **22-1** in Fig. 7)

Mg@Ge$_{10}$ (D_{4d})
Bicapped
square antiprism
42 total electrons
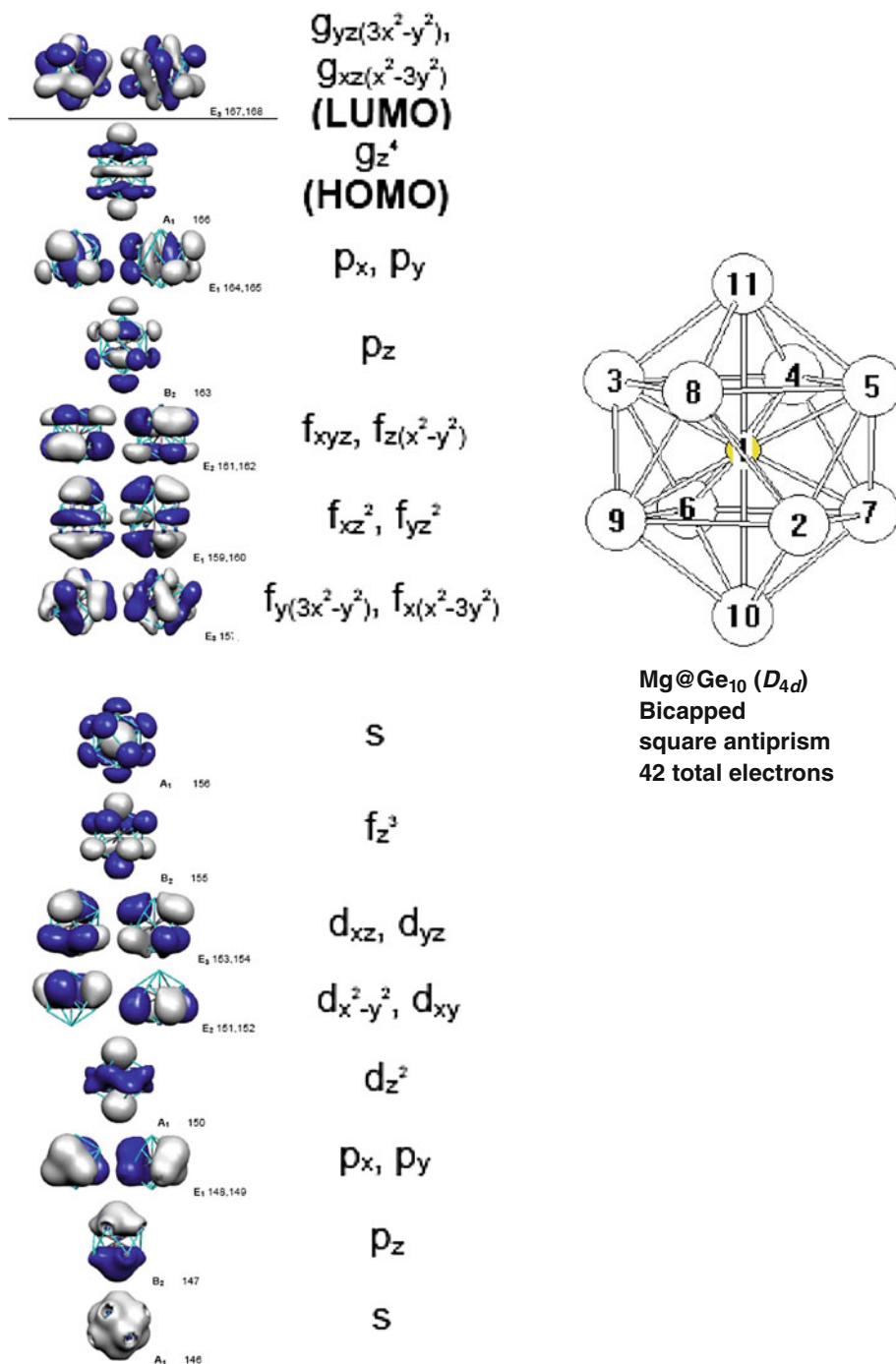
nodes are noted in the three 2p orbitals, which are the highest lying of the 20 orbitals forming the closed {1s, 1p, 1d, 2s, 1f, 2p} shell.

The other polyhedron approximated by a sphere is a C_{3v} polyhedron derived from a tetracapped trigonal prism. This is the $M@In_{10}^{10-}$ polyhedron found experimentally in the $K_{10}In_{10}M$ intermetallics (M = Ni, Pd, Pt) [29]. A related C_{3v} polyhedron is the so-called *isocloso* polyhedron found in metallaboranes such as the ruthenaborane (η^6-Me$_6$C$_6$) RuB$_9$H$_9$ [54]. Since the $M@In_{10}^{10-}$ systems [29] are 40 total electron systems, the isoelectronic 40 total electron dication $Mg@Ge_{10}^{2+}$ was investigated (structure **20-4** in Fig. 6). The 40 total electron configuration is a closed shell configuration (Fig. 3). Consistent with this the molecular

orbitals of C_{3v} $Mg@Ge_{10}^{2+}$ show the expected spherical harmonic ordering with filled 1s, 1p, 1d, 2s, 1f and 2p molecular orbitals leaving no electrons for any 1g orbitals (Fig. 11).

4.2.2 Nonspherical polyhedra

The pentagonal antiprism (Fig. 4) can be derived from a regular icosahedron by removal of a pair of antipodal vertices thereby reducing the symmetry from I_h to D_{5d}. The Wade–Min gos rules [4–7] predict a pentagonal antiprismatic borane to be a $2n + 6$ skeletal electron *arachno* system with the same 26 skeletal electrons as the icosahedron from which it is originally derived. The stable
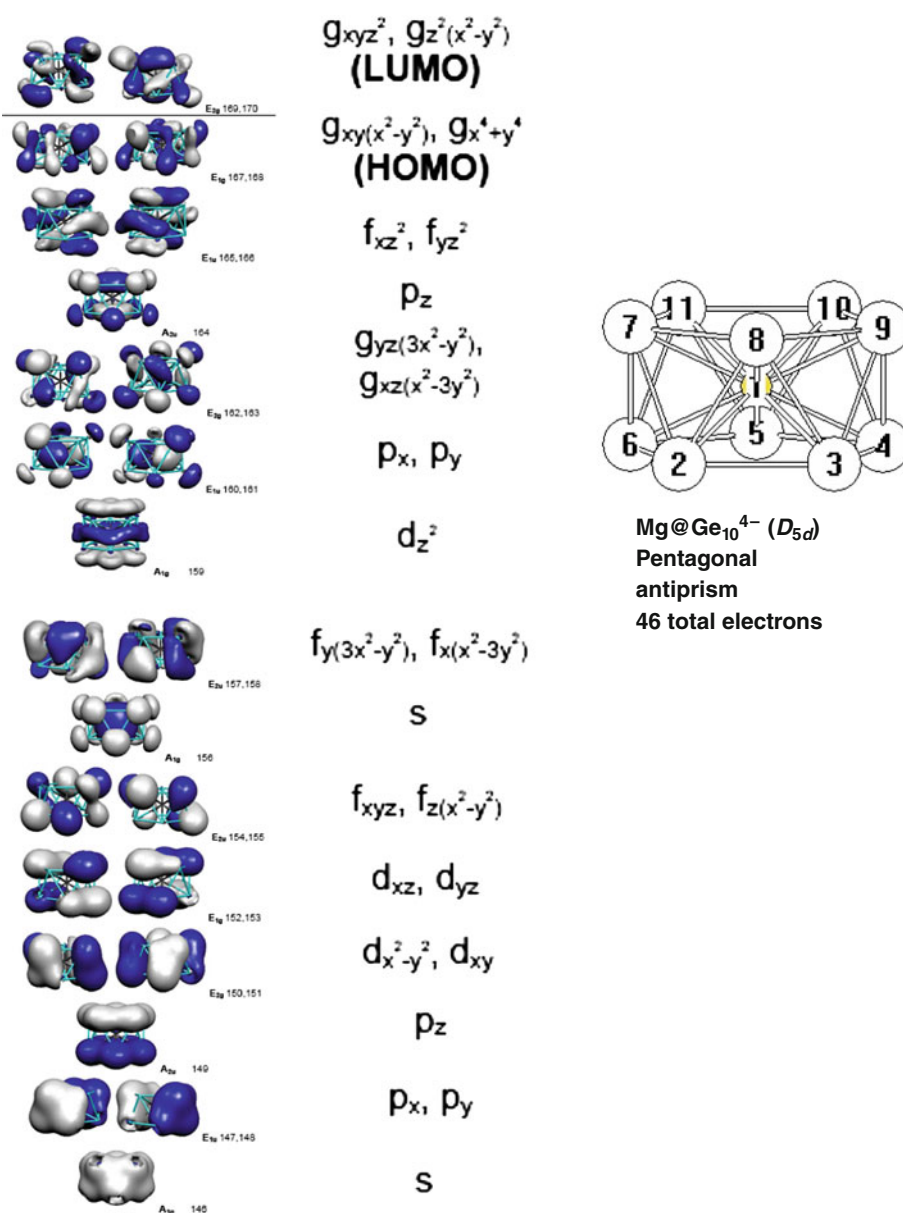
Fig. 11 The bonding molecular orbitals for the 40 total electron C_{3v} $Mg@Ge_{10}^{2+}$ structure (structure **20-4** in Fig. 6)
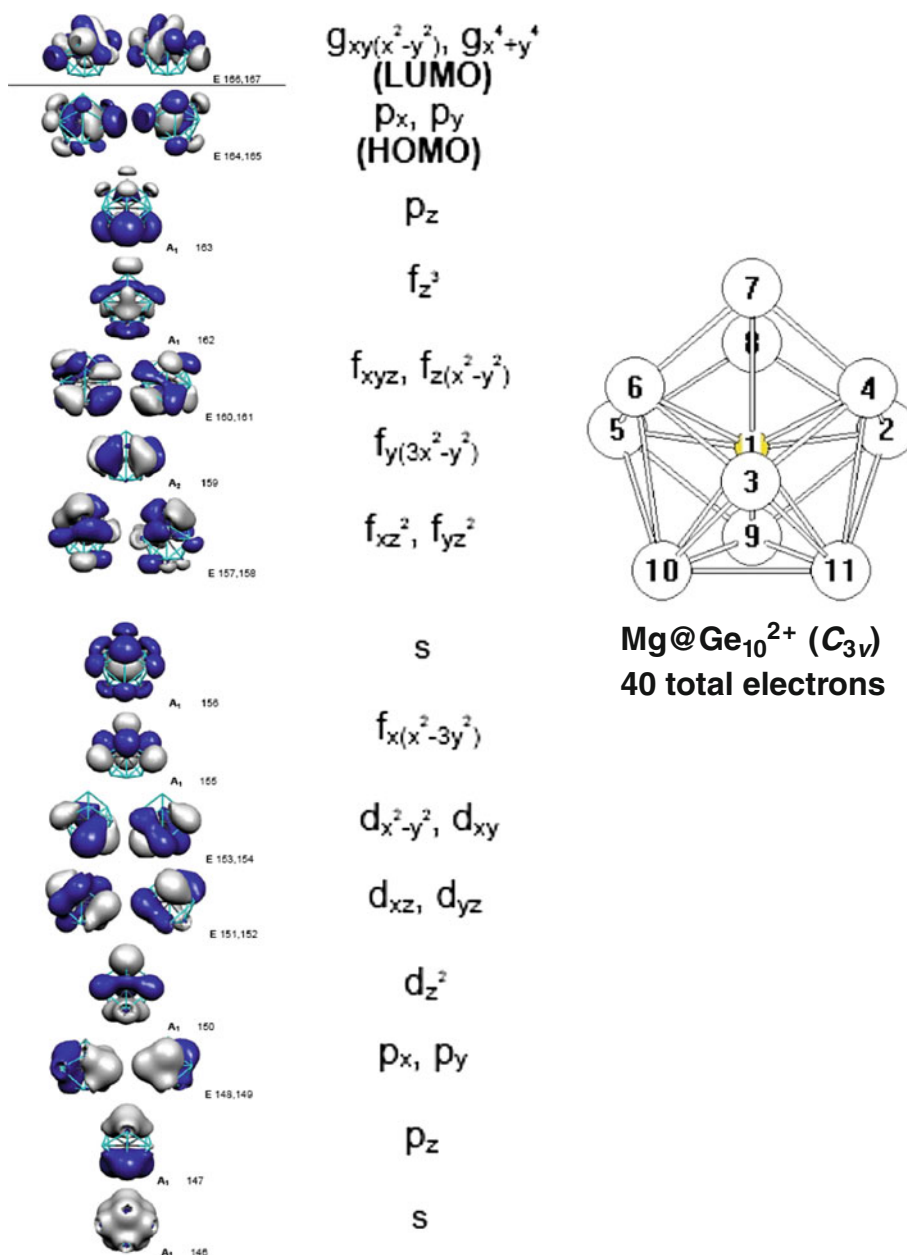
cationic pentagonal antiprismatic bismuth cluster $Pd@Bi_{10}^{4+}$ found in $Bi_{14}PdBr_{16}$ (=$[Pd@Bi_{10}][BiBr_4]_4$) and characterized structurally by X-ray crystallography [34] has the same 26 skeletal electrons since each bare bismuth vertex is a donor of three skeletal electrons leaving an external lone pair. Note that the central palladium atom in $Pd@Bi_{10}^{4+}$ is a zero-electron donor since a neutral palladium atom has no electrons beyond its filled d^{10} shell [31]. Thus $Pd@Bi_{10}^{4+}$ provides an example where the Wade–Mingos rules [4–7] predict the correct structure for a bare post-transition element cluster in contrast to the 8-, 11- and 14-vertex germanium clusters in Fig. 2. An $Mg@Ge_{10}^{4-}$ cluster is isoelectronic with the $Pd@Bi_{10}^{4+}$ cluster and thus was chosen for this study (structure **26-4** in Fig. 9). Note that $Mg@Ge_{10}^{4-}$ has 46 total electrons so that the spherical

harmonic ordering has six 1g electrons in three 1g bonding orbitals in addition to the 40 electrons in the closed {1s, 1p, 1d, 2s, 1f, 2p} shell. However, the $Mg@Ge_{10}^{4-}$ pentagonal antiprism might be expected not to be spherical but instead oblate ellipsoidal (Fig. 5) since it is derived from a spherical polyhedron, namely the icosahedron (Fig. 1), by removal of an antipodal pair of vertices. Figure 12 shows that the pattern of bonding molecular orbitals in $Mg@Ge_{10}^{4-}$ no longer follows the spherical harmonic ordering of Fig. 3. Thus there are four 1g bonding molecular orbitals rather than the three expected from spherical harmonic ordering. In addition the polar $1f(z^3)$ orbital is pushed to such a high energy that it is no longer a bonding molecular orbital. The high energy of the $1f(z^3)$ orbital can be related to the absence of vertex atoms on the C_5 axis of the

Fig. 12 The bonding molecular orbitals for the 46 total electron D_{5d} pentagonal antiprismatic $Mg@Ge_{10}^{4-}$ structure (structure **26-4** in Fig. 9)

g_{xyz^2}, $g_{z^2(x^2-y^2)}$
(LUMO)

$g_{xy(x^2-y^2)}$, $g_{x^4+y^4}$
(HOMO)

f_{xz^2}, f_{yz^2}

p_z

$g_{yz(3x^2-y^2)}$,
$g_{xz(x^2-3y^2)}$

p_x, p_y

d_{z^2}

$f_{y(3x^2-y^2)}$, $f_{x(x^2-3y^2)}$

s

f_{xyz}, $f_{z(x^2-y^2)}$

d_{xz}, d_{yz}

$d_{x^2-y^2}$, d_{xy}

p_z

p_x, p_y

s

Mg@Ge$_{10}^{4-}$ (D_{5d})
Pentagonal
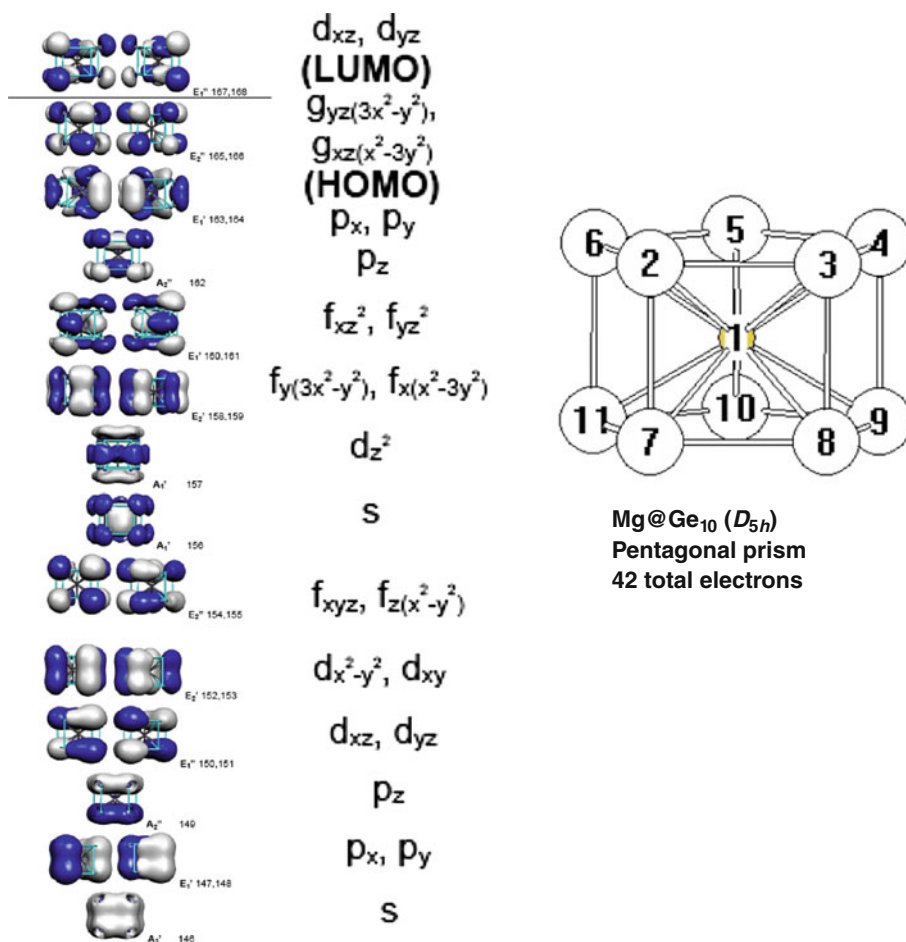**antiprism**
46 total electrons

pentagonal antiprism. The polar d(z^2) orbital, although still a bonding molecular orbital, has an abnormally high energy for the same reason.

The pentagonal prism is also of interest since it is found in the recently discovered transition metal-centered clusters M@Ge$_{10}^{3-}$ (M = Fe [35], Co [36]), which have been structurally characterized by X-ray crystallography. The pentagonal prismatic structures of these clusters with no triangular faces at all were a complete surprise since the polyhedra in almost all other cluster compounds, including all of the clusters treated by the Wade–Mingos rules [4–7], have mainly triangular faces. Although there is some uncertainty in the formal oxidation state of the central metal atom, the diamagnetic cluster Co@Ge$_{10}^{3-}$ can be regarded as a 42 total valence electron system since the interstitial cobalt atom can be considered as a one-electron acceptor to fill its 3d shell corresponding to a formal −1 oxidation state. Thus the neutral D_{5h} pentagonal prismatic Mg@Ge$_{10}$ was used as a model for the Co@Ge$_{10}^{3-}$ cluster. Since the 42 total valence electrons of Mg@Ge$_{10}$ exceeds the magic number of 40 by two electrons, one of the 1g orbitals would be expected to be a filled bonding orbital in the spherical harmonic pattern.

Figure 13 shows that the bonding molecular orbitals of D_{5h} pentagonal prismatic Mg@Ge$_{10}$ (structure **22-3** in Fig. 7), like those of D_{5d} pentagonal antiprismatic Mg@Ge$_{10}^{4-}$ discussed above, do not have the spherical harmonic pattern. In fact, the molecular orbital pattern of the pentagonal prismatic Mg@Ge$_{10}$ has much in common with the molecular orbital pattern of the pentagonal antiprismatic Mg@Ge$_{10}^{4-}$. Of particular note is the missing polar 1f(z^3) orbital among the bonding orbitals in both systems, which is pushed to an energy too high for a bonding orbital. Also in both pentagonal antiprismatic Mg@Ge$_{10}^{4-}$ and pentagonal prismatic Mg@Ge$_{10}$ the lowest energy bonding g molecular orbitals are the same, namely the tropical hexagonal prism {g[$yz(3x^2-y^2)$], g[$xz(x^2-3y^2)$]} pair (Table 2; Figs. 12, 13). Although there is a mismatch in the order of the rotation group of these orbitals (six) with that of the pentagonal prism or antiprism (five), the locations of the lobes of this pair of g orbitals most closely match the vertex locations in the pentagonal prism or antiprism. This match makes the energies of this hexagonal prism set of g orbitals significantly lower than those of any other of the g orbitals.

Fig. 13 The bonding molecular orbitals for the 42 total electron D_{5h} pentagonal prismatic Mg@Ge$_{10}$ structure (structure **22-3** in Fig. 7)

d$_{xz}$, d$_{yz}$
(LUMO)
g$_{yz(3x^2-y^2)}$,
g$_{xz(x^2-3y^2)}$
(HOMO)
p$_x$, p$_y$
p$_z$
f$_{xz^2}$, f$_{yz^2}$
f$_{y(3x^2-y^2)}$, f$_{x(x^2-3y^2)}$
d$_{z^2}$
s
f$_{xyz}$, f$_{z(x^2-y^2)}$
d$_{x^2-y^2}$, d$_{xy}$
d$_{xz}$, d$_{yz}$
p$_z$
p$_x$, p$_y$
s

Mg@Ge$_{10}$ (D_{5h})
Pentagonal prism
42 total electrons

The similarity between the pentagonal prismatic and antiprismatic structures relates to the generation of a pentagonal prism from a pentagonal antiprism by simply rotating one pentagonal face relative to the other pentagonal face by 36°. However, a pentagonal prism is less oblate than the pentagonal antiprism since the two pentagonal faces are further apart in the prism than in the antiprism (compare Figs. 12, 13 for structures with edge lengths as equivalent as possible). This geometrical difference arises from the fact that the edges connecting the two pentagonal faces are parallel with the C_5 axis in the prism but slanted with respect to the C_5 axis in the antiprism.

5 Conclusion

The jellium sphere model [18] has been applied to the bonding molecular orbital ordering in a series of Mg@Ge$_{10}^z$ clusters based on diverse 10-vertex polyhedra exhibiting threefold, fourfold and fivefold symmetries as well as varying degrees of sphericity. In this connection the molecular orbital patterns of the most spherical D_{4d} bicapped square antiprism cluster Mg@Ge$_{10}$ as well as that of an approximately spherical C_{3v} cluster Mg@Ge$_{10}^{2+}$ derived from the tetracapped trigonal prism exhibit the spherical harmonic ordering of the jellium model. In this ordering scheme the 20-orbital {1s, 1p, 1d, 2s, 1f, 2p} shell is filled before any of the 1g molecular orbitals. However, the molecular orbital patterns of the oblate D_{5d} pentagonal antiprism cluster Mg@Ge$_{10}^{4-}$ and the D_{5h} pentagonal prism cluster Mg@Ge$_{10}$ no longer exhibit the spherical harmonic ordering of the jellium model. In these latter clusters the polar $1f(z^3)$ orbital is raised to antibonding levels and the pair of hexagonal prism 1g molecular orbitals become bonding orbitals. These observations suggest that both the D_{4d} bicapped square antiprismatic clusters and the C_{3v} tetracapped trigonal prismatic clusters are spherical enough to be approximated as spheres by the jellium model. However, the oblate D_{5d} pentagonal antiprismatic clusters and the D_{5h} pentagonal prism deviate too much from sphericity for their molecular orbital patterns to correspond strictly to the spherical harmonic pattern predicted by the jellium model.

6 Supporting information available

Tables of distances for the Mg@Ge$_{10}^z$ derivatives ($z = -4$, -2, 0, $+2$); Molecular orbital energies for D_{4d}-Mg@Ge$_{10}$, C_{3v}-Mg@Ge$_{10}^{2+}$, D_{5d}-Mg@Ge$_{10}^{4-}$ and D_{5h}-Mg@Ge$_{10}$; Complete Gaussian 03 Ref. [45].

References

1. Corbett JD (1985) Chem Rev 85:383
2. Corbett JD (1976) Prog Inorg Chem 21:129
3. Williams RE (1971) Inorg Chem 10:210
4. Wade K (1971) Chem Comm 792
5. Wade K (1976) Adv Inorg Chem Radiochem 18:1
6. Mingos DMP (1972) Nat Phys Sci 99:236
7. Mingos DMP (1984) Acc Chem Res 17:311
8. King RB, Heine T, Corminboeuf C, Schleyer PVR (2004) J Am Chem Soc 126:430
9. Schleyer PVR, Maerker C, Dransfeld A, Jiao H, van Eikema Hommes NJR (1996) J Am Chem Soc 118:6317
10. King RB, Silaghi-Dumitrescu I, Kun A (2002) Dalton Trans 3999
11. King RB, Silaghi-Dumitrescu I (2003) Inorg Chem 42:6701
12. King RB, Silaghi-Dumitrescu I, Lupan A (2005) Inorg Chem 44:3579
13. King RB, Silaghi-Dumitrescu I, Lupan A (2005) Dalton Trans 1858
14. King RB, Silaghi-Dumitrescu I, Uţă MM (2006) Inorg Chem 45:4974
15. King RB, Silaghi-Dumitrescu I, Uţă MM (2007) Dalton Trans 364
16. King RB, Silaghi-Dumitrescu I, Uţă MM (2008) Eur J Inorg Chem 3996
17. Dong L, Chen HS, Xie Z (2005) Angew Chem Int Ed Engl 44:2128
18. King RB, Silaghi-Dumitrescu I (2008) Dalton Trans 6083
19. De Heer WA (1993) Rev Mod Phys 65:611
20. Janssens E, Neukermans S, Lievens P (2004) Curr Opin Solid State Mater Sci 8:185
21. Wales DJ, Mingos DMP (1989) Inorg Chem 28:2748
22. Wales DJ, Mingos DMP, Slee T, Zhenyang L (1990) Acc Chem Res 23:17
23. Mingos DMP, Slee T, Zhenyang L (1990) Chem Rev 90:383
24. Stone AJ (1980) Mol Phys 41:1339
25. Stone AJ (1981) Inorg Chem 20:563
26. Stone AJ (1984) Polyhedron 3:1299
27. Bergeron DE, Castleman AW Jr, Morisato T, Khanna SN (2004) Science 304:84
28. Sevov SC, Corbett JD (1991) Inorg Chem 30:4877
29. Henning RW, Corbett JD (1999) Inorg Chem 38:3883
30. Sevov SC, Corbett JC (1993) Inorg Chem 32:1059
31. King RB (2004) Dalton Trans 3420
32. Esenturk EN, Fettinger J, Eichhorn B (2005) Chem Comm 247
33. Esenturk EN, Fettinger J, Eichhorn B (2006) J Am Chem Soc 128:9178
34. Ruck M, Dubenskyy V, Söhnel T (2003) Angew Chem Int Ed 45:2978
35. Zhou B, Denning MS, Kays DL, Goicoechea JM (2009) J Am Chem Soc 132:2802
36. Wang J-Q, Stegmaier S, Fässler TF (1998) Angew Chem Int Ed 2009:48
37. Kumar V, Kawazoe Y (2003) Appl Phys Lett 83:2677
38. Kumar V, Singh AK, Kawazoe Y (2004) Nano Lett 4:677
39. King RB, Silaghi-Dumitrescu I, Uţă MM (2009) J Phys Chem A 113:527

40. King RB, Silaghi-Dumitrescu I, Uţă MM (2009) Inorg Chem 48:8508
41. Vosko SH, Wilk L, Nusair M (1980) Can J Phys 58:1200
42. Lee C, Yang W, Parr RG (1988) Phys Rev B 37:785
43. Becke AD (1993) J Chem Phys 98:5648
44. Stephens PJ, Devlin FJ, Chabalowski CF, Frisch MJ (1994) J Phys Chem 98:11623
45. Frisch MJ et al. (2003) Gaussian 03, Revision A.1. Gaussian, Inc., Pittsburgh (see supporting information for details)
46. Xie Y, Schaefer HF, King RB (2000) J Am Chem Soc 122:8746
47. King RB (2008) J Math Chem 44:5
48. King RB (2005) Polyhedron 1994:13
49. King RB (1997) J Phys Chem A 101:4653
50. Ghosh S, Shang M, Li Y, Fehlner TP (2001) Angew Chem Int Ed 40:1125
51. Wadepohl H (2002) Angew Chem Int Ed 41:4220
52. Le Guennic B, Jiao H, Kahlal S, Saillard J-Y, Halet J-F, Ghosh S, Shang M, Beatty AM, Rheingold AL, Fehlner TP (2004) J Am Chem Soc 126:3203
53. King RB (2006) Inorg Chem 45:8211
54. Littger R, Englich U, Ruhlandt-Senge K, Spencer JT (2000) Angew Chem Int Ed 39:1472